High Frequency Ion Bernstein Wave Heating Experiment
on JIPP T-IIU Tokamak

T. Seki, R. Kumazawa, T. Watari, M. Ono, Y. Yasaka, F. Shimpo, A. Ando,
O. Kaneko, Y. Oka, K. Adati, R. Akiyama, Y. Hamada, S. Hidekuma, S. Hirokura,
K. Ida, A. Karita, K. Kawahata, Y. Kawasumi, Y. Kitoh, T. Kohmoto, M. Kojima,
K. Masai, S. Morita, K. Narihara, Y. Ogawa, K. Ohkubo, S. Okajima, T. Ozaki,
M. Sakamoto, M. Sasao, K. Sato, K.N. Sato, H. Takahashi, Y. Taniguchi,
K. Toi, and T. Tsuzuki

HIGH FREQUENCY ION BERNSTEIN WAVE HEATING
EXPERIMENT ON JIPP T-IIU TOKAMAK

T. SEKI, R. KUMAZAWA, T. WATARI, M. ONO[*], Y. YASAKA[#],

F. SHIMPO, A. ANDO, O. KANEKO, Y. OKA, K. ADATI, R. AKIYAMA,

Y. HAMADA, S. HIDEKUMA, S. HIROKURA, K. IDA, A. KARITA,

K. KAWAHATA, Y. KAWASUMI, Y. KITOH, T. KOHMOTO, M. KOJIMA,

K. MASAI, S. MORITA, K. NARIHARA, Y. OGAWA[†], K. OHKUBO,

S. OKAJIMA[‡], T. OZAKI, M. SAKAMOTO, M. SASAO, K. SATO,

K.N. SATO, H. TAKAHASHI, Y. TANIGUCHI, K. TOI, T. TSUZUKI

National Institute for Fusion Science, Nagoya 464-01, Japan

[*]*Princeton Plasma Physics Laboratory, Princeton,*
New Jersey 08543, U.S.A.

[#]*Faculty of Engineering, Kyoto University, Kyoto 606, Japan*

[†]*Faculty of Engineering, University of Tokyo, Tokyo 113, Japan*

[‡]*College of Engineering, Chubu University, Kasugai 487, Japan*

ABSTRACT

An experiment in a new regime of ion Bernstein wave (IBW) heating has been carried out using 130 MHz high power transmitters in the JIPP T-IIU tokamak. The heating regime utilized the IBW branch between the 3rd and 4th harmonics of the hydrogen ion cyclotron frequencies. This harmonic number is the highest among those used in the IBW experiments ever conducted. The net radio-frequency (RF) power injected into the plasma is around 400 kW, limited by the transmitter output power.

Core heating of ions and electrons was confirmed in the experiment and density profile peaking was found to feature the IBW heating (IBWH). The peaking of the density profile was also found when IBW was applied to the neutral beam injection heated discharges. An analysis by use of a transport code with these experimental data indicates that the particle confinement should be improved in the plasma core region on the application of IBWH.

It is also found that the ion energy distribution function observed during IBWH has less high energy tail than those in conventional ion cyclotron range of frequency heating regimes. The observed IBWH-produced ion energy distribution function is in a reasonable agreement with the calculation based on the quasi-linear RF diffusion / Fokker-Planck model.

1. INTRODUCTION

Due to the excellent accessibility to high temperature and high density plasma core for a relatively wide range of launched parallel index of refraction [1], the ion Bernstein wave heating (IBWH) is well suited for heating reactor plasma core in the future devices. Since IBW can heat the plasma even at higher ion cyclotron harmonics, higher frequency than those in conventional heating regimes in ion cyclotron range of frequency (ICRF) can be used. Furthermore, since the polarization of the wave electric field is in the horizontal direction, IBW may be launched by a lower-hybrid-like waveguide antenna [2]. This makes IBWH more attractive, specifically, in its reactor applications.

In the previous IBWH experiments on JIPP T-IIU, 40 MHz was used. Two heating regimes of physical interest found in the experiment were referred to as Mode-I regime ($\omega = 3/2\Omega_H = 3\Omega_D$) [3] and Mode-II regime ($\omega = \Omega_H = 2\Omega_D$) [4]. In the Mode-I regime, the IBW heating experiment was carried out for the first time in the mid-size tokamak and a strong central ion heating was observed. In the Mode-II experiment, an efficient electron heating was observed. It is predicted theoretically that the wave rays with large $k_\parallel$ out of its spectrum are absorbed via electron Landau damping. In PLT [5-9], the various IBWH regimes ($\omega = 5\Omega_D$, $3/2\Omega_D$, ^{3}He) were identified. The observed ion heating efficiency was comparable to that of the conventional ICRF heating and the particle confinement was improved during IBWH. In Alcator C [10-13], the experiments were performed in the high

density and high toroidal magnetic field regime. The directly launched IBW was detected by the CO_2-laser scattering system. The ion heating and the improvement in the particle confinement during IBWH were also observed. In TNT-A [14-16], which is a small tokamak, antenna loading and wave propagation were investigated in detail and the presence of ion and electron heating regimes was confirmed. However, no appreciable increase of the stored energy has been reported from the recent experiments in JFT-2M [17] and DIII-D [18].

Though the viability of IBWH was demonstrated in many of the experiments, all of these experiments recorded various levels of impurity release during IBWH. In the previous JIPP T-IIU experiment, the injection power was limited by the plasma disruption caused by the impurity influx (thought to be irons from the stainless steel Faraday shields). On PLT, the iron influx from the Faraday shields was successfully reduced by coating the stainless steel shield material with a thin layer of carbon [19]. On DIII-D, the impurity problem was significantly reduced through wall carbonization (on DIII-D, the source of metallic impurity was observed to be mainly from the vacuum vessel wall) [20]. The present JIPP T-IIU experiment is motivated by the hypothesis proposed by Itoh et al. [21]. A particle in the radio-frequency (RF) field has velocity v, energy ε, and excursion length ξ which have following forms:

$$v \cong \frac{qE}{m\omega} \qquad\qquad \varepsilon \cong \frac{1}{2}m(\frac{qE}{m\omega})^2 \qquad\qquad \xi \cong \frac{qE}{m\omega^2} \qquad (1)$$

where q and m are the charge and mass of the particle, and E and ω are the field and frequency of the RF wave, respectively. As the frequency increases, both ξ and ε become small. In the present experiment we choose 130 MHz, which is three times higher than that used in the previous experiments, 40 MHz. Then, it is expected that the particle and/or energy flux which may cause sputtering become smaller, thereby, reducing the influx of impurity. It should be also noted that such non-linear processes as the ponderomotive potential formation which have a similar frequency dependence as Eq.(1) are also reduced by increasing the heating frequency.

We report in this paper the results of the new IBW experiment utilizing higher frequency in JIPP T-IIU. The experimental results are described in section 2. In section 3, the analyses of particle transport is discussed. A new quasi-linear diffusion model of ion energy distribution during IBWH is presented in section 4. The model is used to explain the observed in energy distribution during IBWH. Summary and conclusion are presented in section 5.

2. EXPERIMENTAL RESULTS

Figure 1 shows the cross section of the IBW antennas at the equatorial plane. Each antenna element is a center-fed T shape antenna, so-called Nagoya Type-III coil [22]. This center-fed antenna configuration gives a built-in phasing capability which eliminates the low $n_{\parallel}$ component. The low $n_{\parallel}$ component has more difficulty penetrating into the plasma due to the axial

convective loss effect [23], thereby causing the edge heating and impurity generation. These three antennas are aligned along the toroidal direction at the low field side and protected by the carbon limiters. The whole of antennas are covered by the one unit of double stainless steel Faraday shield.

One of the unique features of this experiment is that it is the highest hydrogen harmonic frequency IBWH experiment ever conducted (ω/Ω_H = 3-4, f ≈ 130 MHz, B_t ≈ 3 T). Figure 2 shows the square of the calculated perpendicular wave number as a function of the major radius for a typical ohmic parameter. In this case, the toroidal magnetic field at R = 0.93 m is 2.85 T and the pure hydrogen plasma is assumed. The resonance layer of the 3rd cyclotron harmonic of hydrogen is located at the plasma center. The 2nd and 4th harmonic layers lie completely outside the plasma. The wave excited at the antenna located in the low field side (the right end of the figure) propagates into the interior of the plasma until absorbed at the resonance layer near the plasma center. In adopting the higher frequency, it is expected that the sputtering at the plasma edge is reduced and the impurity influx would decrease accordingly, as described before. In this experiment, we could inject the IBW power of up to 400 kW without disruption. The power was limited by the transmitter output power and the level is about four times that of the previous 40 MHz IBW experiment. The calculated RF power deposited at the plasma center reached ~ 10 MW/m^3. During IBWH, though the iron influx which is thought to come from the Faraday shields increased, the serious impurity problem which could lead to a major disruption was not encountered. We also searched for

the parametric instabilities [24, 25] with an RF probe but they were not observed.

In optimizing the IBWH performance, it was found that the plasma position control with respect to the antenna position is quite important. The optimum edge density at the antenna position was found to be $\omega \approx \omega_{pi}$, or $n_e \approx 4 \times 10^{17}$ m^{-3} before application of the RF. The plasma tends to disrupt if the antenna edge density is too low or too high. When the plasma is too far away, the RF ponderomotive force can further depress the plasma density in front of the antenna which can lead to the axial convective loss [23]. If the plasma is too close to the antenna, the high plasma density can cause the plasma sheath related problems [26]. Indeed during IBWH, the plasma position control must be preprogrammed to prevent the outward movement (0.5-1.0 cm) of plasma to within few millimeter.

2.1. IBW only injection experiment

To confirm the IBWH in this new heating regime, we launched IBW into an ohmically heated pure hydrogen plasma. Figure 3 shows the time history of a typical shot in which IBW only was applied to the ohmic plasma. At the flat top of the plasma current (= 170 kA), the IBW power of 200 kW is applied (Fig.3(a)). The stored energy measured by the diamagnetic loop increases from 2 kJ to 5 kJ (Fig.3(b)). The electron temperature of the plasma center measured by the electron cyclotron emission (ECE) increases with the injection of IBW (Fig.3(c)) and the sawtooth oscillation is enhanced. The

subsequent decrease of the electron temperature is due to the large increase of the electron density caused by the injection of IBW (Fig.3(e)). The intensity of the H_α line near the antennas decreases during IBWH (Fig.3(d)). H_α signals viewing low field side around the bore limiter increase and those viewing the high field side decrease.

Figure 4 shows the energy spectrum of the hydrogen ions measured by the fast neutral analyzer (FNA). The bulk ion temperature is estimated in the energy range between 1 and 5 keV. In comparison with the ohmic discharge, it is clear that the ions are heated by the injection of IBW. The ion heating is observed also by the Doppler spectroscopy. The central ion temperature obtained from the Fe XXII line reaches $\approx$ 1 keV during IBWH and this is compatible with that of the FNA value. The time history of the bulk ion temperature acquired by the FNA is shown in the Fig.3(f).

Figure 5 is the profile of the electron temperature obtained by the measurement of ECE using the 10 channel polychromator. The polychromator channels are adjusted to give a correct electron temperature profile for a typical ohmic discharge previously given as

$$T_e(r) = T_{e0}(1-(r/a)^2)^2$$

where T_{e0} is the central electron temperature and a is the plasma minor radius. As shown in Fig.5(a), just after the injection of IBW, the temperature near the center of the plasma is raised and the temperature profile peaks at the center. The

central electron temperature reaches ≈ 1.1 keV. As the density increases during IBW, as mentioned before, the whole temperature decreases. We compared this electron temperature evolution with a simulated density rise using the gas puffing as shown in Fig.5(b). When the density rise is produced by the gas puffing the electron temperature goes down as the density increases. Comparing the Fig.5(a) with (b), it is clear that the higher electron temperature is maintained with IBW injection. The electrons are therefore heated during IBWH. However, in this regime, the ray-tracing calculations show predominantly an ion heating.

Figure 6 shows the time evolution of the electron density profile measured by the multi-channel far infrared (FIR) laser interferometer. From this figure, it is found that when IBW is injected the density profile peaks gradually at the center accompanied with the density rise. From such measurements, it is expected that the particle confinement is improved by IBWH particularly in the central region.

Thus, it is found that the central electrons and ions are heated by the injection of IBW alone producing more peaked temperature and density profiles as compared to the ohmic plasma.

2.2. Superposition of NBI and IBW

The superposition of IBWH on neutral beam injection (NBI) presents an interesting heating characteristic. The neutral hydrogen beam of 30 keV and 350 kW is injected tangentially in

the direction of the plasma current (co-injection). The NBI allows the ion temperature profile measurement utilizing the charge exchange recombination spectroscopy (CXRS) [27]. Figure 7 shows the time history of a typical shot when IBW was applied on top of NBI. At the flat top of the plasma current (= 200 kA), NBI (= 350 kW) is injected first and IBW (= 390 kW) is applied shortly after as shown in Fig.7(a). The total input power in this case is about two times the ohmic power. By the injection of NBI and IBW, the stored energy is increased (Fig.7(b)) and the electron temperature at the plasma center is also increased (Fig.7(c)). The H_α signal in the vicinity of the IBW antennas increases by the injection of NBI, but decreases as soon as IBW is injected (Fig.7(d)). H_α signals viewing low field side around the bore limiter increase as well as the case of the IBW only injection. The radiation loss at the plasma center with IBW increased much more than that with NBI (Fig.7(f)). This is mainly due to the increased plasma density ($P_{rad} \propto Z_{eff} n_e^2$). To reduce the radiative losses further, it is clear that the impurity problem must be improved for IBWH. However, the maximum IBWH power injected into the plasma is four times larger than our previous experiment, so the impurity problem in the high frequency regime is successfully reduced. The FNA ion temperature increased with the NBI and IBW, respectively (Fig.7(g)).

Figure 8 shows the profile of the ion temperature measured by CXRS. The increase of the ion temperature by IBW is caused especially in the vicinity of the plasma center and the profile is the center peaked form. This is the remarkable feature in

this experiment. The somewhat higher ion temperature measured by FNA compared with CXRS may be explained by the fact that FNA measured the heated hydrogen ions directly whereas CXRS measured the indirectly heated carbon ion temperature.

Figure 9 is the profile of the electron temperature obtained by the ECE measurements. During the injection of NBI, the electron temperature increases as a whole in comparison with ohmic discharge. When IBW is injected the electron temperature near the plasma center is raised and the profile peaks more. Furthermore, with IBW injection, the central density increases by a factor of 2-2.5.

Figure 10 shows the electron density profile evolution obtained from a multi-channel FIR laser interferometer system using the Abel inversion technique. To obtain a degree of peakedness, the density profile thus obtained is fitted to the following functional form of density profile:

$$n_e(r) = n_{e0}(1-(r/a)^2)^k$$

where n_{e0} is the central electron density and the k is a profile factor. Larger the factor k is, steeper the density profile becomes. Figure 10(a) shows the electron density at the plasma center. Figure 10(b) shows the time evolution of the profile factor k. The indications with arrows in the figures are as follows: P-1 is the period that the plasma is heated ohmically without additional heating. P-2 is the period when only NBI is injected. P-3 is the period that IBW is applied in addition to NBI. P-4 is the period that NBI is turned off but IBW remains

injected into the plasma. When NBI is injected (P-2), the increase of the central electron density is very small and the density profile becomes broad in comparison with the ohmic discharge (P-1). When IBW is injected (P-3), the central electron density increases greatly and the density profile becomes peaky in spite of the broadening effect caused by the NBI. When NBI is turned off and IBW remains applied (P-4), the profile becomes even more peaked than before and the density of the plasma center also increases.

Thus, in superposing on NBI, IBW couples well with the electrons near the plasma center and both the electron temperature and density increase in the plasma central region. The ion temperature is also remarkably raised near the center and the centrally peaked profile is obtained. Due to the combined rise in the central density and temperature, the central plasma energy density is increased remarkably by IBWH. Therefore, the effectiveness of IBWH with the presence of strong NBI heating is demonstrated in this experiment.

3. DISCUSSION OF PARTICLE TRANSPORT ANALYSES

As mentioned before, though NBI is a significant particle source, both the average and central density increase only a little (Fig.7(e) and 10(a)) and the density profile tends to broaden (Fig.10(b)) during NBI. This behavior suggests a reduction in the particle confinement during NBI. In contrast, when IBW is applied, the density profile peaks and the central density increases (Fig.10). Since the particle fueling for IBW

is only taking place at the plasma periphery, this clearly
indicates that the particle confinement in the plasma core
region is improved by the injection of IBW. We estimated the
particle diffusivity by using the following usual particle
transport equation:

$$\frac{\partial n(r)}{\partial t} + \frac{1}{r}\frac{\partial}{\partial r}\left[rV(r)n(r)\right] + \frac{1}{r}\frac{\partial}{\partial r}\left[rD(r)\frac{\partial n(r)}{\partial r}\right] = S(r) \qquad (1)$$

where $n(r)$ is the plasma density, $V(r)$ is the particle
convective velocity which usually flows inward for tokamak
discharges, $D(r)$ is the particle diffusivity, and $S(r)$ is the
particle source term. The particle confinement is improved by
increasing the inward particle convective velocity V or
decreasing the diffusivity D. We solved Eq.(1) for a steady-
state solution. As observed in the previous tokamak
experiments, we use here the value of $V(r)$ twice the Ware-pinch
velocity. For the purpose of comparison, we fix the $V(r)$ and
calculate the corresponding $D(r)$ for the cases being considered
here. Without NBI discharges, $S(r)$ is zero (except at the
edge), and with NBI discharges, $S(r)$ is calculated using the
particle deposition code (NFREYA code). The resulting particle
diffusivity, D $[m^2/s]$, near the plasma center (r ~ 2.6 cm) is
0.035 for the ohmic discharge (P-1 in Fig.10), 0.208 for NBI (P-
2), 0.097 for NBI+IBW (P-3), and 0.025 for IBW (P-4). The
diffusivity during NBI is much larger than that of ohmic
discharge and the particle confinement during NBI deteriorates
considerably from the ohmic discharge. This is consistent with

a typical NBI L-mode discharge. With the injection of IBW, the diffusivity approaches that of ohmic discharge and the confinement is improved. Moreover, when NBI is shut off, the confinement is further improved. It should be noted that the confinement improvements during IBW may be also explained by an increase in the inward convective velocity term instead of the reduction in the diffusivity.

4. DISCUSSION OF QUASI-LINEAR DIFFUSION OF IONS

During IBWH, an interesting feature is observed in the ion energy distribution. Figure 11 shows the energy spectrum of the hydrogen ions for the two representative IBW power levels (as labeled). The high energy tail of the ion distribution produced by IBWH increases as the applied IBW power is increased. However, distinguishable from the fast magnetosonic wave heating case [28], the IBWH-produced high energy ion tail (non-thermal component) does not have the 'runaway' structure; the acceleration tends to stop at a certain energy. We investigated the RF-induced acceleration of ions in the IBW field using the quasi-linear, Fokker-Planck diffusion equation [29, 30].

From Ref.[29], a kinetic equation for the ion distribution function including the quasi-linear heating by RF and Coulomb thermalization is:

$$\frac{\partial f}{\partial t} = C(f) + Q(f) \tag{2}$$

where C(f) is the Coulomb collision term and Q(f) is the quasi-linear diffusion term. Since RF heats the particles perpendicularly, $v_\perp \gg v_\parallel$ and for the electrostatic waves, the wave field is $E_x \approx E$, $E_y \approx 0$. Then from Ref.[30], Q(f) is

$$Q(f) = \frac{\pi Z^2 e^2}{m^2 |k_\parallel|} |E_x|^2 \sum_{n=0}^{\infty} \frac{1}{v_\perp} \frac{\partial}{\partial v_\perp} v_\perp^2 n^2 \frac{|J_n(Z)|^2}{Z^2} \delta[v_\parallel(res)] \frac{1}{v_\perp} \frac{\partial f}{\partial v_\perp} \quad (3)$$

where $J_n(Z)$ is the Bessel function, $Z \equiv k_\perp v_\perp/\Omega_i$, and $v_\parallel(res) \equiv (\omega - n\Omega_i)/k_\parallel$ which is the resonance condition. Since we consider the non-thermal component of the perpendicular velocity distribution, $v_{T_i} \ll v_\perp \ll v_{T_e}$, where $v_{T_j} \equiv (2kT_j/m_j)^{1/2}$, and j denotes the i and e for ions and electrons, respectively. In the RF heating case, the distribution function is distorted in the perpendicular direction, i.e., $\langle v_\perp^2 \rangle \gg \langle v_\parallel^2 \rangle \approx v_{T_i}^2$. After integrated over the $v_\parallel$, Eq.(2) is written in the following form:

$$\frac{\partial f(v_\perp, t)}{\partial t} = -\frac{1}{v_\perp} \frac{\partial}{\partial v_\perp} [\alpha v_\perp f] + \frac{1}{2v_\perp} \frac{\partial^2}{\partial v_\perp^2} [\beta v_\perp f]$$
$$+ \frac{1}{4v_\perp} \frac{\partial}{\partial v_\perp} [\gamma f] + \frac{1}{v_\perp} \frac{\partial}{\partial v_\perp} [K \frac{1}{v_\perp^2} \frac{\partial f}{\partial v_\perp}] \quad (4)$$

where $\alpha \equiv \langle \Delta v_\parallel \rangle + \langle (\Delta v_\perp)^2 \rangle/2v$, $\beta \equiv \langle (\Delta v_\parallel)^2 \rangle$, and $\gamma \equiv \langle (\Delta v_\perp)^2 \rangle$ are given in Ref.[29], and K is a quasi-linear RF diffusion term which is obtained from the Eq.(3). For steady-state, Eq.(4) can be integrated twice and gives the following solution:

$$f(v_\perp) = f(v_{\perp 0}) \exp[-\int_{v_{\perp 0}}^{v_\perp} \frac{-4\alpha v_\perp + 2\beta + 2\beta' v_\perp + \gamma}{2\beta v_\perp + 4K/v_\perp^2} \, dv_\perp] \qquad (5)$$

where the β' denotes the derivative of β with respect to $v_\perp$. For simplicity, we set that the lower bound of the integral, $v_{\perp 0}$, to be twice the ion thermal velocity since we are dealing only the non-thermal component (which is also the experimentally observed value).

From Eq.(3), the velocity dependence of K is given as $K(v_\perp)$ $\propto |J_n(Z)|^2/Z^2$. In the case of IBW, because of the very short wavelength, it is a reasonable approximation to assume Z to be large. Expanding in the large argument limit, noting that $J_n(Z)$ $\propto Z^{-1}$, we obtain $K \propto Z^{-3}$ or $v_\perp^{-3}$ since $Z \propto v_\perp$. One should note here that by assuming a small spread in $k_\parallel$ (≈ 10 % which is easily satisfied in the experiment), the oscillatory behavior of Bessel function averages to zero, recovering $K \propto Z^{-3}$ type behavior. Inspecting the integrand of Eq.(5), the dominant term in the numerator is $-4\alpha v_\perp$ and in the denominator is $4K/v_\perp^2$. Defining $K \equiv K_0 v_\perp^{-3}$, we can integrate Eq.(5) and obtain:

$$f(v_\perp) \approx f(v_{\perp 0}) \exp[-\frac{v_\alpha^3}{K_0 t_s} (\frac{v_\perp^2}{2} + \frac{v_\perp^5}{5v_\alpha^3})] \qquad (6)$$

where t_s is the slow down time due to the electron drag given in Ref.[29]. As can be seen in Eq.(6), the relevant velocity range can be divided into two regions: $v_\perp < v_\alpha$ and $v_\perp > v_\alpha$ where $E_\alpha = mv_\alpha^2/2 \approx 14.8 \, kT_e$. When $v_\perp \approx v_\alpha$, the power dissipated by the bulk ions equals that by the bulk electrons. Therefore, for $v_\perp < v_\alpha$, the dominant thermalization is by ions and the velocity

distribution assumes a Maxwellian-like form with an effective ion temperature $\propto K_0$ which is proportional to the RF power. In this regime, since v_α^3 and τ_s are both proportional to $T_e^{3/2}$, there is no dependence on electron temperature. For $v_\perp > v_\alpha$, the $v_\perp^5/v_\alpha^3$ electron drag term rapidly start to dominate the ion drag term. In this regime, the electron dissipation which is independent of the fast ion energy is quite effective in counteracting the RF diffusivity which decreases rapidly with $v_\perp^{-3}$. Therefore, it can be concluded that the IBW heated distribution function tends to assume the Maxwellian characteristic up to v_α and then decreases more rapidly above v_α.

From the experimental point of view, this property indicates that if the RF power density is not sufficiently high, the resulting distribution is very much like Maxwellian distribution since the charge-exchange fast neutral signal falls well below the noise level before reaching v_α. However, if the RF power density is sufficiently high, the steeper drop in the distribution function near v_α should be observable. In Fig.12, we plot the calculated distribution using Eq.(6). The best agreement with experiment is obtained when the RF power density is chosen 2 and 10 MW/m^3 for 90 and 360 kW case, respectively. For the 90 kW case, the observed energy distribution function is Maxwellian-like. For the 360 kW case, the rapid fall off starts around 15 keV which is in the same range as $E_\alpha \approx 15$ keV with $T_e \approx 1$ keV. The agreement between the ion tail behavior and the present theoretical model appears to be reasonable.

5. CONCLUSION

IBWH investigation was extended on JIPP T-IIU, utilizing high power 130 MHz transmitters, to the $3\Omega_H$-$4\Omega_H$ range which is the highest hydrogen harmonics to date. Investigation in the high harmonic frequency range is important because it can lead to an early waveguide antenna experiment for IBWH as planned for FTU [31]. A three-element phased antenna array was used to launch a relatively well defined $n_{\parallel}$ spectrum with $n_{\parallel} \approx 4$-8. With the increase of frequency from the previous 40 MHz to 130 MHz, the maximum input power could be increased to 400 kW, which is four times larger than the previous value. The 130 MHz experiment has much less impurity problem than the 40 MHz case which could be due to the combination of higher frequency and antenna phasing. It should be noted that both 40 MHz and 130 MHz IBWH experiments utilized antennas with stainless steel Faraday shields. When IBWH is applied, the profile of electron density peaks in the core region of the plasma, suggesting an core particle confinement improvement. Similarly, an increase of the central ion and electron temperatures is observed. The core confinement improvement and central heating by IBWH are also observed when IBW is combined with NBI. From plasma transport analyses, it is found that the particle confinement is improved in the plasma core region with application of IBWH. This confinement improvement persisted even with NBI heating. If the mechanism of the confinement improvement can be clarified, it might lead to a method to actively control the plasma transport by IBWH.

As the IBWH power is increased, an interesting non-thermal tail formation has been observed. The high energy ion tail produced by IBWH does not have the run-away feature as often produced in the fast magnetosonic wave ICRF heating experiments. Instead, the IBWH-produced ion tail tends to stop at certain energy range. To explain the observed ion tail features, we have developed a quasi-linear RF diffusion / Fokker-Planck model for IBWH. The model appears to agree well with the observed ion energy distribution. In particular, the rapid decrease of RF diffusion above the electron-ion equi-dissipation energy, $E_\alpha \approx 15 \ kT_e$, can be explained with this model. The present model confirms the bulk ion heating nature of IBWH. This heating model also predicts a favorable fusion reaction yield by IBWH since for a reactor situation where temperature is sufficiently high, $T_e \geq 10$ keV, any ion acceleration beyond E_α tends to reduce the fusion reactivity and fusion power amplification factor Q.

As for the future plan, due to the importance of tokamak transport for the fusion program, it would be worthwhile to investigate the cause of the plasma transport improvement during IBWH. This improvements may be related to the fluctuation suppression by poloidal velocity shear created by IBWH [32]. To measure plasma fluctuation and potential, a multi-channel FIR laser scattering system and a 0.5 MeV heavy ion beam probe are in preparation. To reduce the metallic impurity influx, the stainless steel Faraday shields will be coated with a thin carbon layer as in PLT [19], which should further reduce the radiative losses during IBWH. Minimization of radiative loss

channel is of course very important to access actual improvement of plasma energy confinement during IBWH.

REFERENCES

[1] ONO, M., STIX, T.H., WONG, K.L., HORTON, T., in Plasma
    Physics and Controlled Nuclear Fusion Research 1980 (Proc.
    8th Int. Conf. Brussels, 1980), Vol.2, IAEA, Vienna (1981)
    501.

[2] KAKO, E., ANDO, R., ICHIMURA, M., et al., Fusion Technology
    12 (1987) 293.

[3] ONO, M., WATARI, T., ANDO, R., et al., Phys. Rev. Lett. **54**
    (1985) 2239.

[4] OGAWA, Y., KAWAHATA, K., ANDO, R., et al., Nucl. Fusion **27**
    (1987) 1379.

[5] WILSON, J.R., and the PLT Group, in RF Plasma Heating
    (Proc. 6th Top. Conf. Callaway Gardens, GA, 1985) 28.

[6] HOSEA, J.C., WILSON, J.R, HOOKE, W., et al., Plasma Phys.
    Control. Fusion **28** (1986) 1241.

[7] WILSON, J.R., BELL, R., CAVALLO, A., et al., Nucl. Matt.
    145-147 (1987) 616.

[8] ONO, M., BEIERSDORFER, P., BELL, R., et al., in Plasma
    Physics and Controlled Nuclear Fusion Research (Proc. 11th
    Int. Conf. Kyoto, 1986), Vol. 1, IAEA, Vienna (1987) 477.

[9] ONO, M., BEIERSDORFER, P., BELL, R., et al., Phys. Rev.
    Lett. **60** (1988) 294.

[10] TAKASE, Y., MOODY, J.D., FIORE, C.L., et al., Phys. Rev.
     Lett. **59** (1987) 1201.

[11] PORKOLAB, M., BONOLI, P., CHEN, KUOIN, et al., in Plasma
     Physics and Controlled Nuclear Fusion Research 1986 (Proc.
     11th Int. Conf. Kyoto, 1986), Vol. 1, IAEA, Vienna (1987)
     509.

[12] MOODY, J.D., PORKOLAB, M., FIORE, C.L., et al., Phys. Rev. Letters **60** (1988) 298.

[13] MOODY, J.D., PORKOLAB, M., Phys. Fluids B1 (1989) 1675.

[14] SHINOHARA, S., NAITO, O., UEDA, Y., TOYAMA, H., MIYAMOTO, K., J. Phys. Soc. Jpn. **55** (1986) 2648.

[15] SHINOHARA, S., NAITO, O., MIYAMOTO, K., Nucl. Fusion **26** (1986) 1097.

[16] SHINOHARA, S., NAITO, O., TOYAMA, H., MIYAMOTO, K., in Applications of Radio-Frequency Power to Plasmas (Proc. 7th Top. Conf. Kissimmee, FL, 1987) 330.

[17] TAMAI, H., OGAWA, T., MATSUMOTO, H., ODAJIMA, K., JFT-2M GROUP, in Radio-Frequency Power in Plasmas (Proc. 8th Top. Conf. Irvine, CA,1989), American Physical Society, New York (1989) 350.

[18] PINSKER, R.I., MAYBERRY, M.J., PORKOLAB, M., PRATER, R., in Radio-Frequency Power in Plasmas (Proc. 8th Top. Conf. Irvine, CA, 1989), American Physical Society, New York (1989) 314.

[19] TIMBERLAKE, J., COHEN, S., GREENE, G.J., ONO, M., WILSON, J.R., Bull. Am. Phys. Soc. **31** (1986) 1467.

[20] PINSKER, R.I., MAYBERRY, M.J., PETTY, C.C., et al., in Radio-Frequency Power in Plasmas (Proc. 9th Top. Conf. Charleston, SC, 1991), American Physical Society, New York (1991) 105.

[21] ITOH, K., FUKUYAMA, A., ITOH, S.-I., Comments on Plasma Phys. and Controlled Fusion. 10 (1986) 91.

[22] WATARI, T., HATORI, T., KUMAZAWA, R., et al., Phys. Fluids **21** (1978) 2076;

WATARI, T., ADATI, K., AOKI, T., et al., Nucl. Fusion **22** (1983) 1359.

[23] ONO, M., in Radio-Frequency Power in Plasmas (Proc. 9th Top. Conf. Charleston, SC, 1991), American Physical Society, New York (1991) 223.

[24] PORKOLAB, M., BERNABEI, S., HOOKE, W.M., MOTLEY, R.W., NAGASHIMA, T., Phys. Rev. Letters **38** (1977) 230.

[25] VAN NIEUWENHOVE, R., VAN OOST, G., BEUKEN, J.-M., et al., in Controlled Fusion and Plasma Heating (Proc. 15th Eur. Conf. Dubrovnik, 1988), Vol. 12B, Part II, European Physical Society (1988) 778.

[26] PERKINS, F.W., Nucl. Fusion **29** (1989) 583.

[27] IDA, K., HIDEKUMA, S., Rev. Sci. Instrum. **60** (1989) 867.

[28] SEKI, T., KUMAZAWA, R., TAKASE, Y., et al. Nucl. Fusion **31** (1991) 1369.

[29] STIX, T.H., Nucl. Fusion 15 (1976) 737.

[30] KENNEL, C.F., ENGELMANN, F., Phys. Fluids **9** (1966) 2377.

[31] CARDINALI, A., CESARIO, R., DE MARCO, F., ONO, M., in Controlled Fusion and Plasma Physics (Proc. 16th Eur. Conf. Venice, 1989), Vol. 13B, Part III, European Physical Society (1989) 1069.

[32] BIGLARI, H., ONO, M., DIAMOND, P.H., CRADDOCK, G.G., in Radio-Frequency Power in Plasmas (Proc. 9th Top. Conf. Charleston, SC, 1991), American Physical Society, New York (1991) 376.

FIGURE CAPTIONS

Fig.1.   The structure of the IBW antennas, the Faraday
          shields and the carbon protectors.

Fig.2.   The dispersion relation of IBW for the hydrogen
          plasma. The abscissa is the major radius and the
          ordinate is the square of the perpendicular wave
          number. Electron temperature of the plasma center and
          edge are 900 eV and 90 eV, respectively. Ion
          temperature of the plasma center and edge are 350 eV
          and 35 eV, respectively. Electron density of the
          plasma center and edge are 1×10^{19} m^{-3} and 1×10^{18}
          m^{-3}, respectively.

Fig.3.   Time history of the typical shot in the case of the
          IBW only: (a) applied IBW power. (b) stored energy.
          (c) central electron temperature. (d) the intensity
          of the H_α signal near the antennas. (e) average
          electron density. (f) ion temperature.

Fig.4.   Energy spectrum of the hydrogen ions before and after
          the injection of IBW.

Fig.5.   Electron temperature profiles.
          (a) Electron temperature profiles of ohmic (OH)
          phase, just after the IBW injection($\overline{n_e}$ = 1×10^{19}
          m^{-3}), and after a while ($\overline{n_e}$ = 3×10^{19} m^{-3}) are shown.
          (b) For comparison, the density rise induced by the
          injection of IBW is simulated by the gas puffing.

Fig.6.   Time evolution of the electron density profile during
          IBW.

Fig. 1

Fig. 2

$\omega = 3\omega_{cH} \rightarrow$

$\leftarrow$ center

Fig. 3

Fig. 4

Fig. 5

Fig. 6

Fig. 7

(a) IBW Power [MW]
IBW
NBI

(b) Stored Energy [kJ]

(c) Electron Temperature [keV]

(d) Hα [arb. unit]

(e) Average Density [10^{18}/m^3]

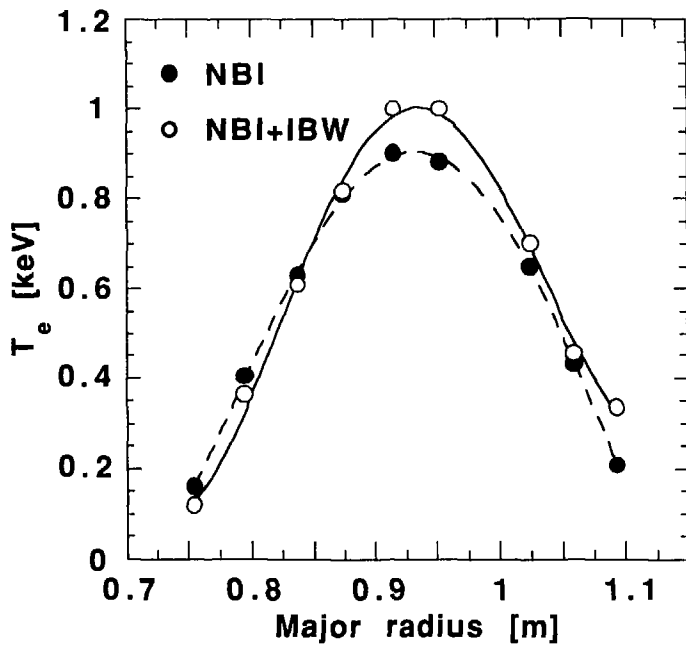(f) Radiation loss [arb. unit]

(g) Ion Temperature [keV]

Time [ms]
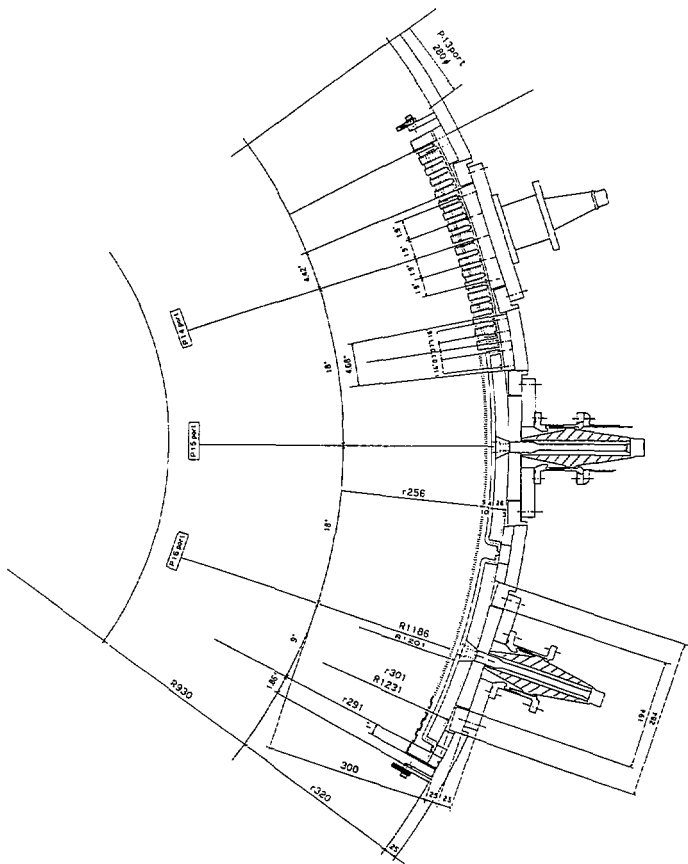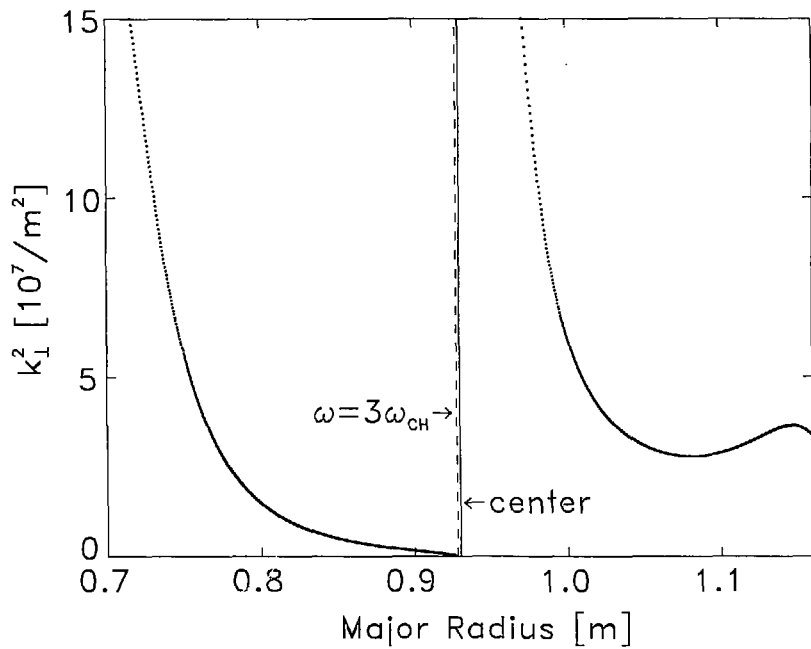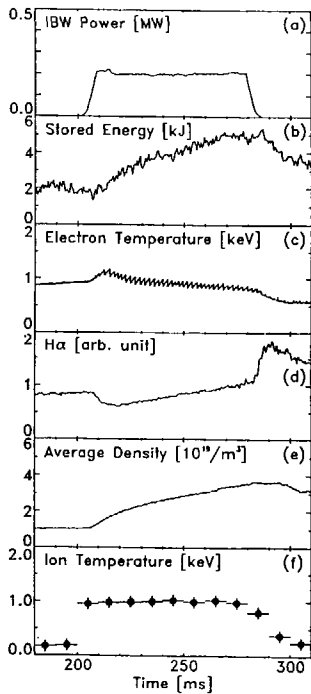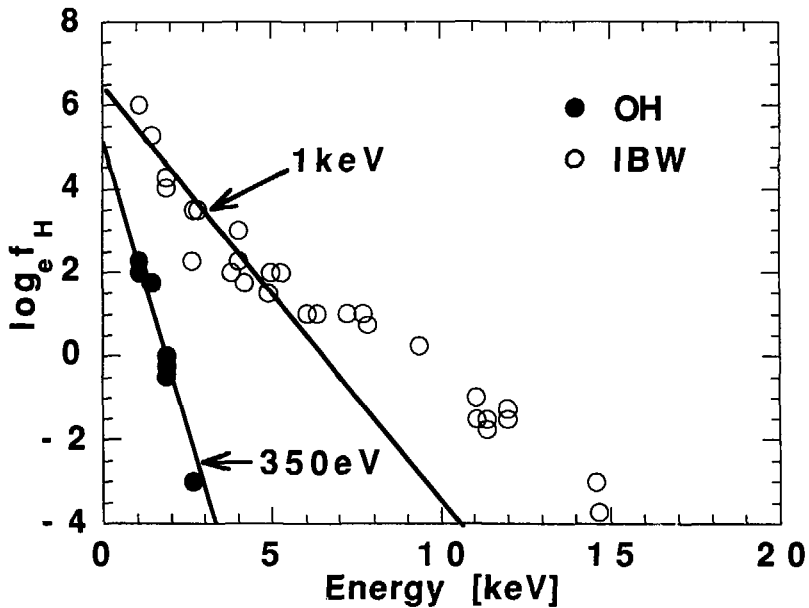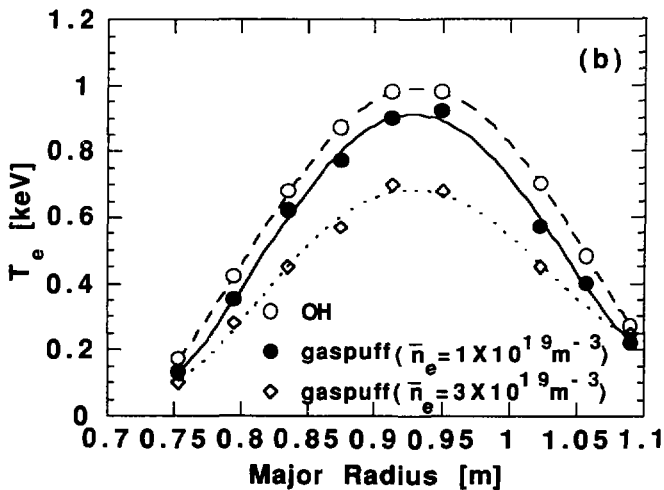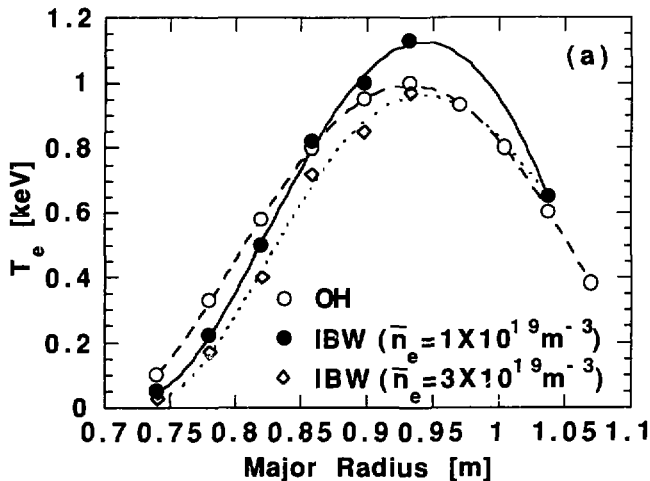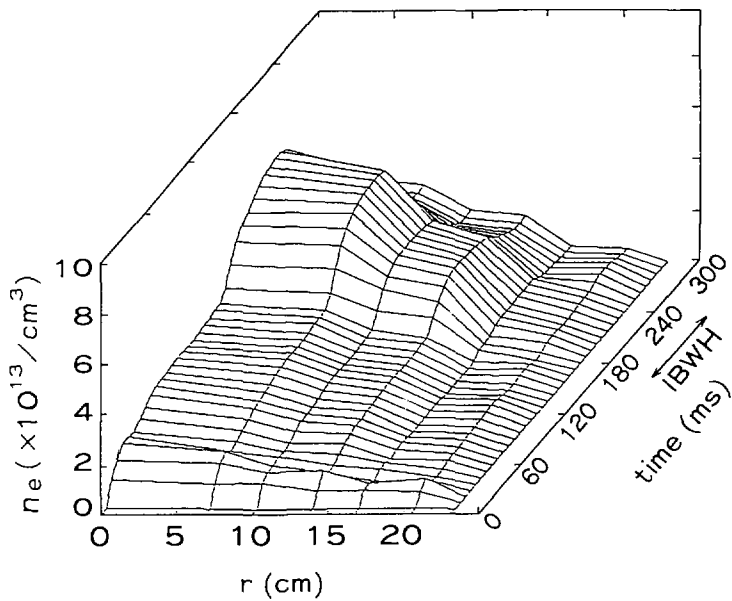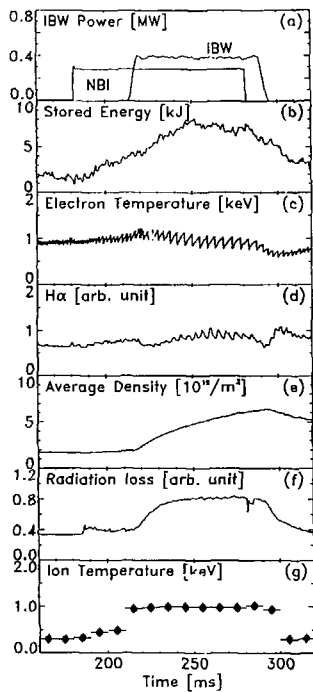
Fig. 8
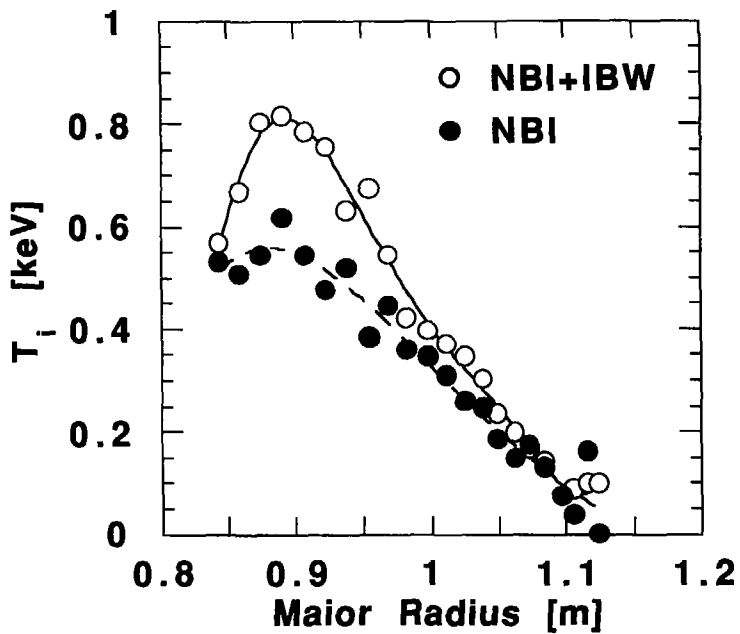
Fig. 9
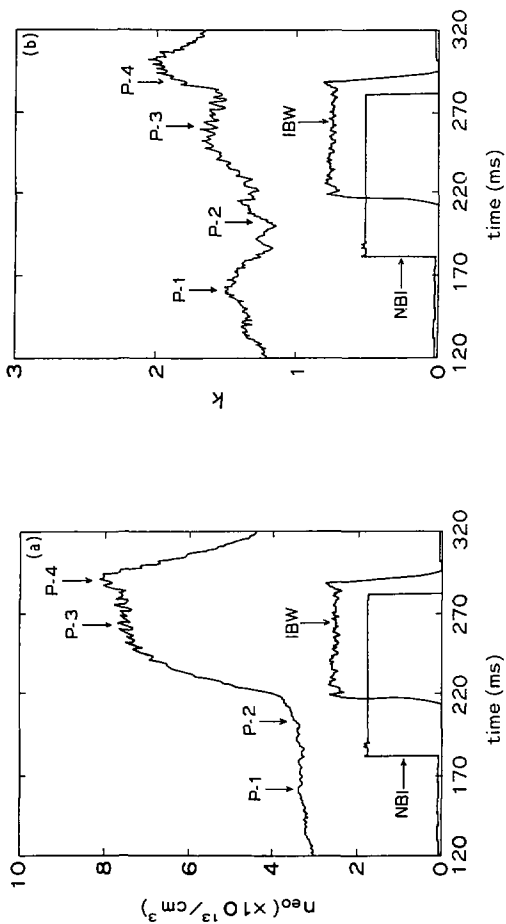
Fig. 10
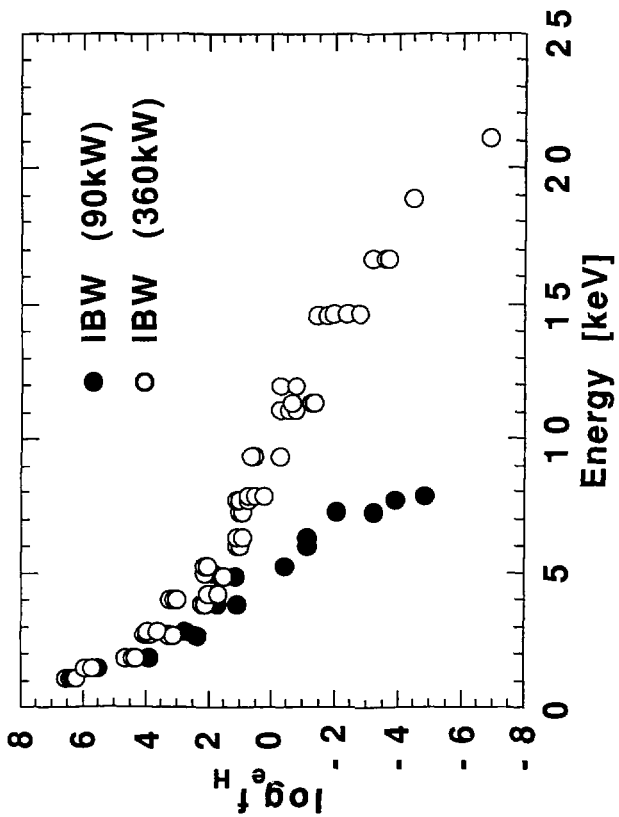
Fig. 11

Fig. 12
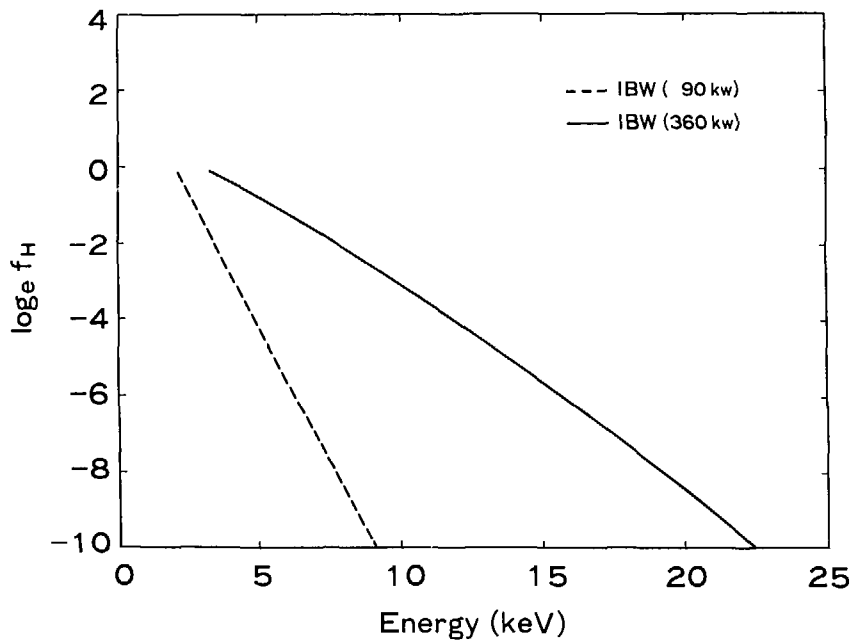
Recent Issues of NIFS Series

NIFS-125   H. Sugama and M. Wakatani, *Statistical Analysis of Anomalous Transport in Resistive Interchange Turbulence* ;Dec. 1991

NIFS-126   K. Narihara, *A Steady State Tokamak Operation by Use of Magnetic Monopoles* ; Dec. 1991

NIFS-127   K. Itoh, S. -I. Itoh and A. Fukuyama, *Energy Transport in the Steady State Plasma Sustained by DC Helicity Current Drive* ;Jan. 1992

NIFS-128   Y. Hamada, Y. Kawasumi, K. Masai, H. Iguchi, A. Fujisawa, JIPP T-IIU Group and Y. Abe, *New Hight Voltage Parallel Plate Analyzer* ; Jan. 1992

NIFS-129   K. Ida and T. Kato, *Line-Emission Cross Sections for the Charge-exchange Reaction between Fully Stripped Carbon and Atomic Hydrogen in Tokamak Plasma*; Jan. 1992

NIFS-130   T. Hayashi, A. Takei and T. Sato, *Magnetic Surface Breaking in 3D MHD Equilibria of l=2 Heliotron* ; Jan. 1992

NIFS-131   K. Itoh, K. Ichiguchi and S. -I. Itoh, *Beta Limit of Resistive Plasma in Torsatron/Heliotron* ; Feb. 1992

NIFS-132   K. Sato and F. Miyawaki, *Formation of Presheath and Current-Free Double Layer in a Two-Electron-Temperature Plasma* ; Feb. 1992

NIFS-133   T. Maruyama and S. Kawata, *Superposed-Laser Electron Acceleration* Feb. 1992

NIFS-134   Y. Miura, F. Okano, N. Suzuki, M. Mori, K. Hoshino, H. Maeda, T. Takizuka, JFT-2M Group, S.-I. Itoh and K. Itoh, *Rapid Change of Hydrogen Neutral Energy Distribution at L/H-Transition in JFT-2M H-mode* ; Feb. 1992

NIFS-135   H. Ji, H. Toyama, A. Fujisawa, S. Shinohara and K. Miyamoto *Fluctuation and Edge Current Sustainment in a Reversed-Field-Pinch*; Feb. 1992

NIFS-136   K. Sato and F. Miyawaki, *Heat Flow of a Two-Electron-Temperature Plasma through the Sheath in the Presence of Electron Emission*; Mar. 1992

NIFS-137   T. Hayashi, U. Schwenn and E. Strumberger, *Field Line Diversion Properties of Finite β Helias Equilibria*; Mar. 1992

NIFS-138   T. Yamagishi, *Kinetic Approach to Long Wave Length Modes in Rotating Plasmas*; Mar. 1992

NIFS-139   K. Watanabe, N. Nakajima, M. Okamoto, Y. Nakamura and M. Wakatani, *Three-dimensional MHD Equilibrium in the Presence of Bootstrap Current for Large Helical Device (LHD)*; Mar. 1992

NIFS-140   K. Itoh, S. -I. Itoh and A. Fukuyama, *Theory of Anomalous Transport in Toroidal Helical Plasmas*; Mar. 1992

NIFS-141   Y. Kondoh, *Internal Structures of Self-Organized Relaxed States and Self-Similar Decay Phase*; Mar. 1992

NIFS-142   U. Furukane, K. Sato, K. Takiyama and T. Oda, *Recombining Processes in a Cooling Plasma by Mixing of Initially Heated Gas*; Mar. 1992

NIFS-143   Y. Hamada, K. Masai, Y. Kawasumi, H. Iguchi, A. Fijisawa and JIPP T-IIU Group, *New Method of Error Elimination in Potential Profile Measurement of Tokamak Plasmas by High Voltage Heavy Ion Beam Probes*; Apr. 1992

NIFS-144   N. Ohyabu, N. Noda, Hantao Ji, H. Akao, K. Akaishi, T. Ono, H. Kaneko, T. Kawamura, Y. Kubota, S. Morimoto. A. Sagara, T. Watanabe, K. Yamazaki and O. Motojima, *Helical Divertor in the Large Helical Device*; May 1992

NIFS-145   K. Ohkubo and K. Matsumoto, *Coupling to the Lower Hybrid Waves with the Multijunction Grill*; May 1992

NIFS-146   K. Itoh, S. -I.Itoh, A. Fukuyama, S. Tsuji and Allan J. Lichtenberg, *A Model of Major Disruption in Tokamaks*; May 1992

NIFS-147   S. Sasaki, S. Takamura, M. Ueda, H. Iguchi, J. Fujita and K. Kadota, *Edge Plasma Density Reconstruction for Fast Monoenergetic Lithium Beam Probing*; May 1992

NIFS-148   N. Nakajima, C. Z. Cheng and M. Okamoto, *High-n Helicity-induced Shear Alfvén Eigenmodes*; May 1992

NIFS-149   A. Ando, Y. Takeiri, O. Kaneko, Y. Oka, M. Wada, and T. Kuroda, *Production of Negative Hydrogen Ions in a Large Multicusp Ion Source with Double-Magnetic Filter Configuration*; May 1992

NIFS-150   N. Nakajima and M. Okamoto, *Effects of Fast Ions and an External Inductive Electric Field on the Neoclassical Parallel Flow, Current, and Rotation in General Toroidal Systems*; May 1992

NIFS-151   Y. Takeiri, A. Ando, O. Kaneko, Y. Oka and T. Kuroda, *Negative Ion*

Extraction Characteristics of a Large Negative Ion Source with Double-Magnetic Filter Configuration; May 1992

NIFS-152   T. Tanabe, N. Noda and H. Nakamura, *Review of High Z Materials for PSI Applications* ; Jun. 1992

NIFS-153   Sergey V. Bazdenkov and T. Sato, *On a Ballistic Method for Double Layer Regeneration in a Vlasov-Poisson Plasma*; Jun. 1992

NIFS-154   J. Todoroki, *On the Lagrangian of the Linearized MHD Equations*; Jun. 1992

NIFS-155   K. Sato, H. Katayama and F. Miyawaki, *Electrostatic Potential in a Collisionless Plasma Flow Along Open Magnetic Field Lines*; Jun. 1992

NIFS-156   O.J.W.F.Kardaun, J.W.P.F.Kardaun, S.-I. Itoh and K. Itoh, *Discriminant Analysis of Plasma Fusion Data*; Jun. 1992

NIFS-157   K. Itoh, S.-I. Itoh, A. Fukuyama and S. Tsuji, *Critical Issues and Experimental Examination on Sawtooth and Disruption Physics*; Jun. 1992

NIFS-158   K. Itoh and S.-I. Itoh, *Transition to H-Mode by Energetic Electrons*; July 1992

NIFS-159   K. Itoh, S.-I. Itoh and A. Fukuyama, *Steady State Tokamak Sustained by Bootstrap Current Without Seed Current*; July 1992

NIFS-160   H. Sanuki, K. Itoh and S.-I. Itoh, *Effects of Nonclassical Ion Losses on Radial Electric Field in CHS Torsatron/Heliotron*; July 1992

NIFS-161   O. Motojima, K. Akaishi, K. Fujii, S. Fujiwaka, S. Imagawa, H. Ji, H. Kaneko, S. Kitagawa, Y. Kubota, K. Matsuoka, T. Mito, S. Morimoto, A. Nishimura, K. Nishimura, N. Noda, I. Ohtake, N. Ohyabu, S. Okamura, A. Sagara, M. Sakamoto, S. Satoh, T. Satow, K. Takahata, H. Tamura, S. Tanahashi, T. Tsuzuki, S. Yamada, H. Yamada, K. Yamazaki, N. Yanagi, H. Yonezu, J. Yamamoto, M. Fujiwara and A. Iiyoshi, *Physics and Engineering Design Studies on Large Helical Device*; Aug. 1992

NIFS-162   V. D. Pustovitov, *Refined Theory of Diamagnetic Effect in Stellarators*; Aug. 1992

NIFS-163   K. Itoh, *A Review on Application of MHD Theory to Plasma Boundary Problems in Tokamaks*; Aug. 1992

NIFS-164   Y.Kondoh and T.Sato, *Thought Analysis on Self-Organization Theories of MHD Plasma*; Aug. 1992